An experimentally-driven approach to model bending in a thermally activated SMA-based beam

A. Fortini, R. Rizzoni, A. Suman, E. Fabbri, M. Merlin, M. Pinelli

Department of Engineering University of Ferrara, via Saragat 1, 44122 Ferrara, Italy

Abstract

In this paper, the bending behavior of an active SMA-based beam, made up of a NiTi alloy strip externally joined to a PA66-GF30 polymeric lamina, is examined. Firstly, experimental investigations were conducted in a purpose-built test bench where a forced airflow promoted the reverse and forward phase transformations of the NiTi strip via heating and cooling ramps. The macroscopic shape changes associated with the shape memory effect deforms the structure in the cantilevered condition. The evolution of the shape memory behavior was investigated via digital image analysis, performed at both the end of heating and the end of the thermal cycle on cooling. Next, a theoretical prediction combining the classical beam model for bending with the assumption of incomplete recovery upon cooling was developed. The theoretical results indicate good agreement with experimental data showing how the proposed approach can be effectively used to predict the behavior in bending of SMA-based actuator working in controlled recovering condition.

List of symbols

Latin letters

A	Austenite phase
A_S, A_F	Austenitic start/finish temperature
C_A, C_M	Stress influence coefficient at the onset/end of the martensitic plateau
E_A, E_M	Young's modulus of austenite/martensite
E_S, E_P	Young's modulus of SMA/polymer
I_S, I_P	Second moment of inertia of SMA/polymer
M	Martensite phase (multi-variant)
M_S, M_F	Martensitic start/finish temperature
m	Bending moment
N	Number of training cycles
n	Number of actuation cycles
R	Curvature radius
R_M, R_R	Maximum/residual curvature radius
S	Martensite phase (single-variant)
s	Arc-length coordinate
T	Temperature
t	Time
v	Transversal displacement
w	Axial displacement

Greek letters

ε_L	Maximum recoverable strain
σ_S, σ_F	Critical stress of start/finish detwinning
δ	Deflection
δ_M, δ_R	Maximum/residual deflection
X	Curvature
X_M, X_R	Maximum/residual curvature
X_i	Initial curvature (after shape-setting)
X_0	Curvature of the stress-free SMA strip
φ	Angular rotation
ξ	Martensite volume fraction

Acronyms

CAD	Computer-Aided Design
DSC	Differential Scanning Calorimetry
HDT	Heat Deflection Temperature
SME	Shape Memory Effect
SMAs	Shape Memory Alloys
TWSME	Two-way Shape Memory Effect
TTRs	Transformation Temperatures

Subscript

S	SMA strip
P	Polymeric lamina

Keywords: actively controlled structures, shape memory alloys (SMA), bending, cantilever beam

1. Introduction

Shape memory alloys (SMAs) are a class of fascinating metallic materials endowed with the capability to recover seemingly permanent strains through temperature-induced phase changes. As the material is deformed in the martensitic phase (M), the thermally-activated crystalline transformation into the austenitic phase (A) promotes the recovery of the original memorized shape, via the so-called Shape Memory Effect (SME).

The combination of the unique characteristics of SMAs, due to the thermoelastic martensitic phase transformation, with the structural properties of other materials, typically polymers or polymer-based composites, has provided the large-scale development of smart structures with improved and optimized mechanical properties and functionalities [1,2]. Benefits of SMA-based active structures rely on the high recoverable strains (up to 10 %) and high power-to-weight ratio of the SMA component combined with the elastic behavior of the host material. The active element usually works in the so-called controlled recovery condition since the SMA material is partially restrained from recovering its original shape [3,4]. Depending upon the actuation mode required for the intended application, SMA active elements can be in the form of helical springs [5–8], wires [9–11], rods [12–14], strips [15–18], sheets or ribbons [19]. Due to the large amount of force and displacement produced on heating, SMAs are used for sensing, actuation or self-healing purposes [3,20] in different branches of engineering including aerospace devices [21–23], civil structures [24,25] and biomedical applications [26–28].

In literature there are several examples of adaptive engineering devices working in bending and in which the active element could be embedded [29], inserted [17,30,31] or externally-connected [32] to the host matrix. To promote the flexural activation of the device by means of embedded active elements, SMA wires are the most widely adopted. They are usually prestrained under tensile loading conditions and placed away from the neutral axis [29]. For the embedding strategies, the issues include the manufacturing process [33,34], the SMA-resin interface strength [35–37], the stress transfer [38] and the modeling [39] of such structures. Considering the efforts necessary to ensure the adhesion among active elements and the matrix [37], these actuating solutions remain a challenging problem. As effective alternatives, non-embedding approaches, taking advantage of the bending shape recovery of SMA elements, have been proposed. Baz et al. [17] investigated buckling and vibration behaviors of a flat structure equipped with NiTi strips, thermally trained to memorize controlled transverse deflection, arranged inside sleeves of a glass-epoxy structure. Chandra [31] considered the use of SMA bender elements, trained to memorize bending shape, in graphite-epoxy and kevlar-epoxy composite beams. This analysis was conducted to study the bending and twisting displacements of a bending-torsion coupled composite spar intended to twist a rotor blade. Yang et al. [32] examined the shape control of a composite structure with SMA actuators externally-connected to the surface by bolt-joint connectors and they presented a first-order model to predict the shape deformations of the hybrid composite. Dealing with inserted or externally-connected active elements working in bending, a specific shape-setting treatment must be performed. The optimization of the heat treatment parameters is one of the most important challenges to achieve the proper bent shape on actuation [40]. Some general guidelines and practical details about shape-setting of Nitinol can be found in [41] and process conditions as well as the modeling concerning shape-setting in [42–44]. Nevertheless, tailoring both the memorized shape and the parameters should be specifically and experimentally determined [45,46].

Owing to the widespread applications of SMAs as active materials in the so-called active flexible structures, a considerable amount of literature has been concerned with the development of comprehensive constitutive models [1,47]. To provide reliable predictions, SMAs modeling has usually to face with large-scale motions, related structural non-linear equations and SMA non-linear constitutive laws. As a result, constitutive models derived from thermodynamical or micromechanical principles include mathematical complexity and non-availability of microstructural material parameters, which impair their use in practical and convenient design purposes. In this paper, we focus the attention on phenomenological one-dimensional models as they can capture better than three-dimensional ones many of the special features that characterize the one-dimensional behavior of SMAs, avoiding too complex formulations and open up the possibility of analytical solutions or FEM analysis [48–51]. Moreover, the development of active SMA-based structures comprises complex design strategies usually requiring a deep knowledge of the intrinsic non-linear and hysteretic behavior of SMA, the structural and geometrical specifications of both the active and the host medium, the integration mode, the expected performance, i.e. force and displacement values, the actuation and control strategies, the constraint conditions as well as the effective modeling approach. For some comprehensive design approaches the reader is referred to [3,4,41].

In previous works by the authors [16,52,53] the performance of a SMA-based morphing blade intended for an automotive axial fan has been experimentally and numerically investigated. This novel application has been tested in a purpose-built test bench, which indicated the efficacy of the airflow thermal actuation. Based on these research activities, it is very important to find a model to predict the curvatures of the device during activation of the SMA elements. Hence, the motivation of the present work is to develop an experimentally-driven model to grasp, in a simple but effective way, the phenomena involved in the activation process. To do so, we propose a simple but original theoretical prediction which combines the classical beam model for

bending with the assumption of incomplete recovery upon cooling. This latter assumption is based on Brinson's results for restrained recovery in traction [48]. The model parameters have a clear physical meaning and they have been set by performing suitable standard tests. The ability of the model to reproduce the experimental bending behavior of the SMA-active cantilever is assessed and the proposed theoretical prediction is found to be in good agreement with the experimental data. The main contribution of the present paper is thus expected to provide practitioners and engineers with an easy-to-use analysis tool for practical implementations and optimized exploitation of SMAs.

This paper is structured as follows. Section 2 provides the material selection, for both the SMA strip and the polymeric lamina, as well as the description of the purpose-built facilities and the experimental tests approaches. Section 3 collects the experimental findings for both thermomechanical training and actuation cycles, while Section 4 presents the analytical approach which, starting from Brinson's analysis [48], introduces the description of the bending behavior through a phenomenological constitutive model for the controlled recovery case. Section 5 and Section 6 comprise the experimental validation of the assumptions and the discussion of the main results, respectively. In Section 7 the main concluding remarks with possible future developments and perspectives are collected.

2. Materials and methods

2.1 Materials selection

The experiments and the associated analytical approach described in the present paper deal with the analysis of the bending behavior of a SMA-coupled structure made up of a NiTi-based strip, externally joined to a polymeric lamina. Firstly, the thermomechanical training of the SMA strip was achieved by 50 consecutive cycles, whereas the performance of the SMA-coupled structure was investigated through further 30 thermal actuation cycles.

Concerning the active SMA strip, a NiTi shape memory alloy (Memry Metalle Company, Bethel, CT, USA), of the nominal composition $Ni_{50.2}Ti_{49.8}$ at. %, was chosen. Among the commercially available ones, the alloy with a nominal A_F temperature being low enough to be attainable through air heating was selected. Starting from a 1 mm thick plane foil, several strips were cut to a dimension of 90 mm x 1 mm x 1 mm by means of electro-erosion machining. Transformation temperatures (TTRs) were evaluated by Differential Scanning Calorimetry (DSC) analyses performed, through a DSC-TA Instrument Q2000, on a small portion of the material. TTRs values, extrapolated from the DSC thermograms, are summarized in Tab. 1. The mechanical properties of the SMA material (Tab. 1) were investigated by uniaxial tensile tests, performed at 25 °C and 150 °C, under displacement controlled loading conditions by using an Instron type machine with a 500 N load cell. Tests performed at 25 °C let to estimate the Young modulus of the martensite, E_M, the transformation stresses at the onset and at the end of the martensitic plateau, σ_S and σ_F respectively, and the maximum recoverable strain, ε_L. At the same time, the Young modulus of the austenite, E_A, was estimated at 150 °C. More details concerning both DSC and tensile tests can be found in [42].

Table 1 - Properties of the NiTi alloy: TTRs and mechanical specifications.

Parameter	Value	Parameter	Value
Martensitic start temperature (M_S)	69 °C	Young's modulus of martensite (E_M)	28423 MPa
Martensitic finish temperature (M_F)	46 °C	Stress at the onset of the martensitic plateau (σ_S)	149 MPa
Austenitic start temperature (A_S)	82 °C	Stress at the end of the martensitic plateau (σ_F)	210 MPa
Austenitic finish temperature (A_F)	104 °C	Maximum recoverable strain (ε_L)	0,06
		Young's modulus of austenite (E_A)	63475 MPa

Based on the calorimetric results, a tailored shape-setting treatment was tuned to memorize a proper bent shape. The SMA strip was strained in the martensitic state, to shape an arc of a circle with a uniform curvature by wounding it on a cylindrical jig. This fixture was then placed into a tube furnace at 450 °C for 25 min in constrained conditions in order to prevent the shape recovery on heating, and quenched in water at 25 °C. The memorized arc showed a curvature radius of 25,08 mm, corresponding to an initial curvature X_i of 0,04 mm^{-1}. Shape-setting temperature and time parameters were chosen according to the experimental results of a previous study, which indicate that shaping at 450 °C for 25 min leads to an optimized shape recovery behavior [42].

With regards to the polymer, an injected molded 30 % glass fiber reinforced Polyamide 66 (PA66-GF30) was used, in form of laminae of 90 mm x 10 mm x 1.5 mm. The material specifications, provided by the manufacturer, are listed in Tab. 2. As shown, the selected compound enabled to investigate the bending behavior of the SMA-based beam as the maximum operating temperature is well above the A_F value. Likewise, mechanical properties of the polymer let the system to be soft enough to provide large deformation induced by SMA strip on heating as well as stiff enough of being capable of self-recovery on cooling.

Table 2 - Mechanical and thermal properties of the polymeric compound (data sheet supplied by manufacturer).

Parameter	Value	Parameter	Value
Tensile modulus at 23 °C (ISO 527-2:2012)	10000 MPa (dry) 7200 MPa (conditioned)	Vicat softening temperature (ISO 306:2013)	250 °C
Yield stress (crosshead of 50 mm/min)	190 MPa	Deflection temperature 1.8 MPa (HDT-A) (ISO 75-2:2013)	240 °C
Flexural modulus at 23 °C (ISO 178:2010)	9000 MPa (dry) 6500 MPa (conditioned)	Max service temperature	240 °C
Flexural strength (ISO 780:2015)	265 MPa (dry) 210 MPa (conditioned)		

2.2 Experimental setup

Thermal actuation was achieved by a forced airflow, obtained inside a purpose-built test bench, composed of a convergent device and a polymethyl methacrylate transparent measurement section (Fig. 1a). A tailored holding system, displayed in the blow-up of Fig. 1b, was placed inside the measurement section, towards the flow direction. This fixture enabled to provide the cantilevered configuration during tests for both the sole SMA strip (namely free recovery condition) and for the SMA-coupled structure (namely controlled recovery condition).

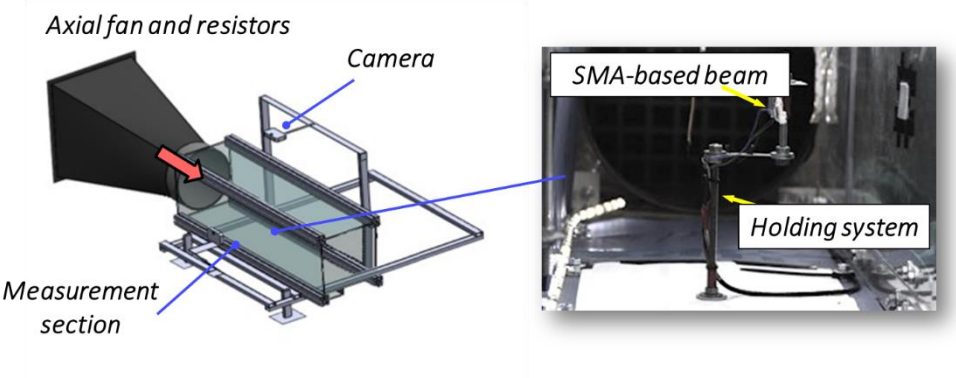

(a) (b)

Figure 1 – Test bench employed for the actuation cycles.

An axial fan with a nominal 1500 m^3/h flow rate pulled and forced the airflow through resistors employed for heating and through the measurement section. Such an apparatus led to a time-wise thermal gradient of up to about 6 °C/min in heating mode and up to about 9 °C/min in cooling mode. Several calibrated thermocouples were installed in the measurement section to monitor and acquire temperature trends of the airflow, the SMA and the polymer. Hot airflow led the temperature of the SMA to rise from room temperature up to 105 °C, promoting the reverse phase transformation (M→A) whose recovery stresses are responsible for the bending deformation. Likewise, the forward phase transformation (A→M) was achieved by forced convection to 35 °C, as the resistors were switched off.

2.3 Bending behavior assessment

Thanks to the transparency of the measurement section, the shape evolution was continuously evaluated via digital image analysis from the camera acquisitions (Fig. 1). In particular, in order to control the shape

changes associated with the temperature trend, video and temperature acquisitions were synchronized. The bending behavior was quantitatively determined via a CAD software reconstruction of several frames extracted from the recorded video, which enabled to quantify both the deflection, δ, and the curvature radius, R (Fig. 2). The measurements were done by considering visual markers drawn on the SMA strip and on the PA66-GF30 lamina. This methodology was applied for the reconstruction of both SMA strip training cycles and SMA-based beam actuation cycles described in Section 2.4.

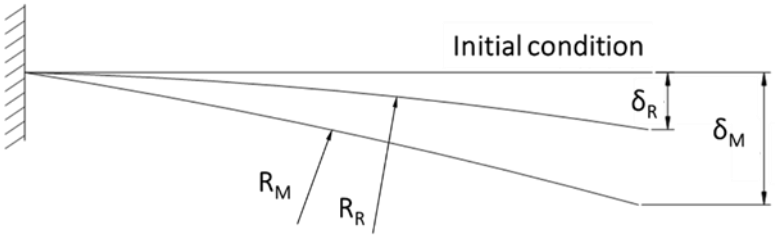

Figure 2 – Schematic illustration of the beam configuration before and after thermal actuation.

With regard to deflection and curvature parameters depicted in Fig. 2, analyses were conducted on the video frames extracted at the peak temperature on heating (named maximum deflection, δ_M) and at the end of the thermal cycle (named residual deflection, δ_R). Deflection values were evaluated taking the initial time frame in the undeformed position (named initial condition) as a reference. Similarly, curvature values were designated as X_M and X_R, respectively.

2.4 SMA-based structure

The tested SMA-based structure was made by externally joining the SMA strip to the polymeric lamina through two zip ties located at its mid-length and at its one end, respectively. The other end was fixed to prevent all the degree of freedom. The test system configuration along with the indication of the above-described elements is depicted in Fig. 3.

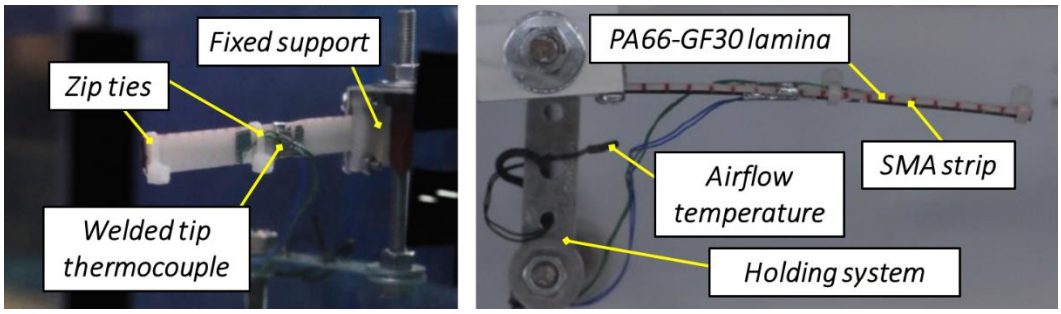

(a) (b)

Figure 3 – Set-up used during bending actuation of the SMA-based beam in the cantilevered configuration: (a) side view and (b) top view.

As stated, prior to the join with the polymeric lamina, the SMA strip was firstly trained by means of 50 consecutive thermomechanical cycles and then the SMA-based beam was actuated by further 30 consecutive thermal actuation cycles. Each cycle consisted of consecutive heating and cooling ramps in the 35 °C – 105 °C temperature range.

3. Results

3.1 SMA strip training cycles

Thermomechanical training comprised a controlled deformation of the material followed by a thermal cycle by repeating the sequence of deformation at a temperature below M_F and free recovery at zero stress by an airflow at a temperature above A_F. After the shape-setting treatment, the SMA strip was firstly strained at

$T<M_F$ by wounding it on a steel cylinder, whose radius enables to reach, after spring-back, the flat shape. Starting from this configuration, actuation was achieved in the test bench by a heating/cooling ramp, as reported in the diagram of Fig. 4. As an example, in Fig. 4 the experimental temperature trends against time for the 1st training cycle, evaluated for both the airflow (in gray) and the SMA strip (in black), are depicted. As shown, the measurement system provides uniform thermal conditions of the airflow stream which results in an overall actuation time of about 900 s. In Fig. 4, the effect of strip deflection on SMA strip temperature variation is clearly visible. Taking into consideration the temperature trend of SMA strip, the curvature variation that occurs from 200 s to 450 s is due the strip deflection and the consequent modification of the thermal input in the proximity of the strip. Figure 4 also reports some video frames extracted from the recorded video during the heating ramp of the 1st actuation cycle, including the corresponding time instant and temperature values. From these snapshots, it appears the progressive SMA-based beam deflection as the temperature increases.

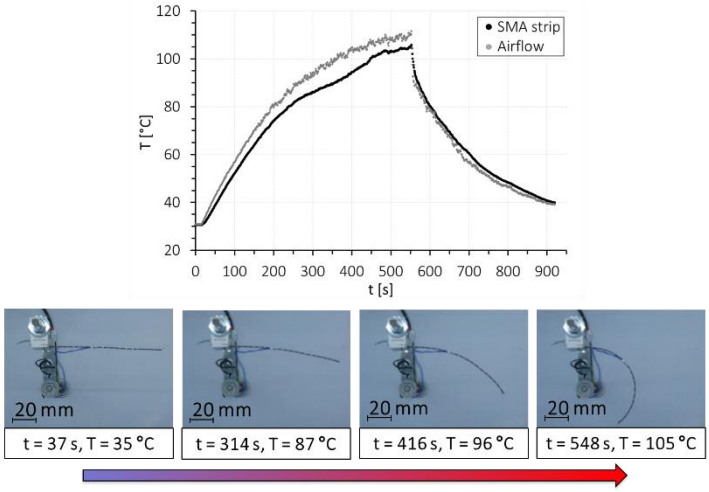

Figure 4 – Temperature-time trends of the 1st training cycle with the associated video frames sequence of the heating ramp.

To examine the influence of the training sequence on the SME, the quantitative analysis of the bending motion, based on CAD software reconstruction of the shape, is proposed. The curvature evolution as a function of temperature, during the 1st, 10th, 20th, 30th, 40th and 50th cycle is given in Fig. 5. The arrows indicate the heating and the cooling ramp, respectively, whereas the horizontal dashed line indicates the initial curvature X_i of 0,04 mm^{-1} obtained after shape-setting. Taking into account the curvature value of the 1st cycle evaluated at 105 °C, it appears the partial recovery of the memorized shape with respect to X_i, with a loss of about 25 %. In addition, during the firsts 20 cycles, the maximum achievable curvature values show noteworthy variations on increasing the number of training cycles. With respect to the highest curvature reached during the 1st cycle of 0,03 mm^{-1}, this value decreases up to beneath 0,015 mm^{-1} after 20 cycles. The material response significantly changes up to about the 30th cycle, whereupon there is a gradual stabilization and repeatability of the curvature trends, as shown in Fig. 5.

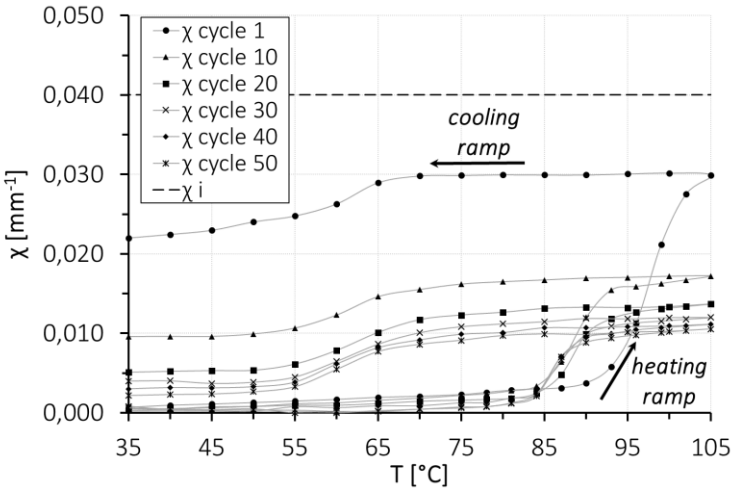

Figure 5 – SMA strip training cycles: curvature-temperature evolution for the 1st, 10th, 20th, 30th, 40th and 50th cycle.

3.2 SMA-based structure actuation

The actuation of the SMA-based structure comprised 30 consecutive thermal cycles, of which the first corresponds to the 51st of the SMA strip and to the 1st of the PA66-GF30 lamina. To repeatedly actuate the structure in bending, heating/cooling ramps were performed. As for the thermomechanical training cycles, the heating ramp ends as the temperature of the SMA strip reaches 105 °C and the subsequent cooling ramp ends when the strip is at 35 °C. Figure 6 provides the experimental temperature trends as a function of time, evaluated for the airflow (in gray), the SMA strip (in green) and the PA66-GF30 lamina (in black). As can be seen, the temperature gradients in both the SMA and the polymer are quite similar and consistent with the airflow temperature evolution. Comparable trend variations occur, similar to those described in the previous section. Given the uniform thermal conditions of the airflow stream and the high reproducibility of the temperature trends on the structure, the depicted trends are representative for all the thermal cycles. Figure 6 reports also the video frames extracted at initial condition, maximum deflection and residual deflection instants.

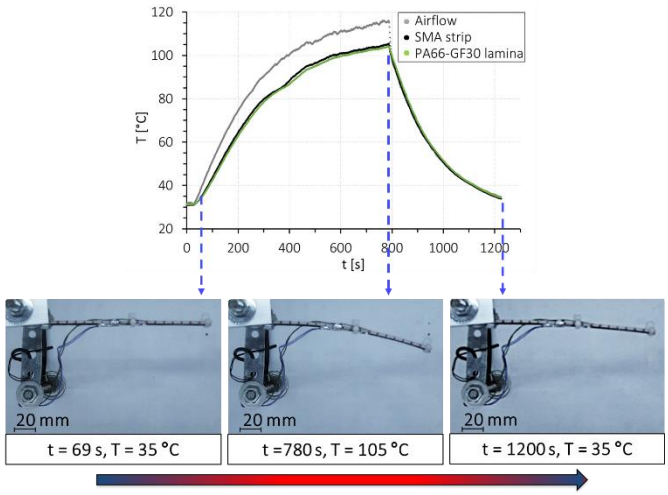

Figure 6 – Thermal actuation of the SMA-coupled structure: temperature-time trends with the associated video frames at initial condition, maximum deflection and residual deflection instants.

To evaluate the effect of the polymer on the hysteretic behavior of the SMA, Fig. 7 reports the comparison among the 50th training cycle of the SMA strip in free recovery condition (cross markers) and the 1st and the 2nd actuation cycles of the SMA-based structure (circle and triangle markers, respectively). The figure shows a clear and remarkable reduction of the maximum achievable curvature on heating due to the presence of the polymer. The curvature obtained at the end of the heating ramp for the sole SMA strip is about 0,01 mm^{-1} whereas for the structure is of 0,004 mm^{-1}. During the heating ramp, the curvature of the sole SMA (cross

markers) is small before 80 °C and, once the temperature exceeds the austenitic start temperature, a noteworthy increase of the curvature values is observed. From about 95 °C the curvature values keep increasing up to the peak temperature and the slope becomes approximatively asymptotic. During the subsequent cooling ramp, the curvature trend shows a significant change in slope at about 70 °C, as expected from the TTRs values (Tab. 1). At the end of the entire cycle, the material exhibits a residual curvature of about 0,002 mm^{-1} that indicates some residual deformation that could not fully be recovered on cooling. Considering the 1st actuation cycle of the SMA-based structure (circle markers), the maximum achievable curvature and the associated hysteresis decrease. As expected, due to the polymer stiffness, the TTRs are shifted to higher temperatures with respect to the free recovery condition (Tab. 1). Besides, at the end of the cooling ramp the structure does not completely recover its undeformed flat shape and thus the starting point of the 2nd actuation cycle corresponds to a residual curvature value of 0,01 mm^{-1}. This leads to a remarkable reduction of the hysteresis associated to the actuation cycle and to the complete recovery of the initial shape at the end of the second cooling ramp.

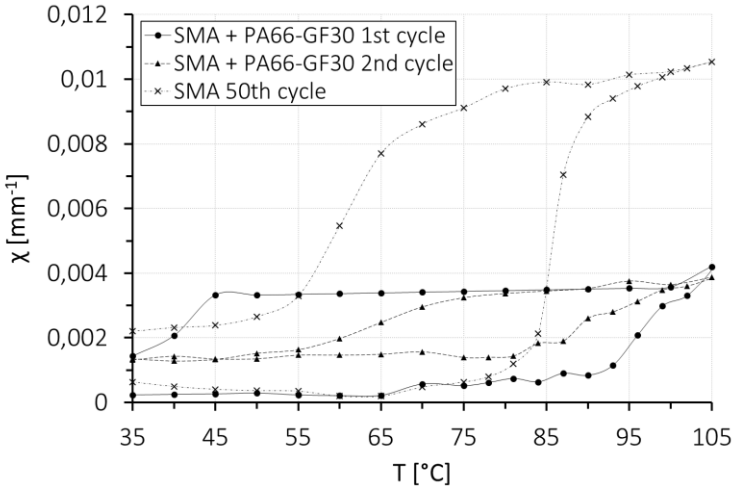

Figure 7 – Curvature-temperature evolution for the 1st and 2nd thermal actuation cycles of the SMA-based structure in comparison with the 50th training cycle of the SMA strip.

4. Theoretical prediction of controlled recovery

To provide an analytical description of the bending behavior of the SMA-based structure tested in Section 3, the following assumptions are made: prior to assembly, the mean lines of the polymeric lamina and of the SMA strip are rectilinear, all curvatures and strains are small, the components are inextensible, shear and torsion deformations are neglected, the zip ties connecting the elements are rigid, thermal expansion is neglected and the temperature is uniformly distributed along the two elements. During heating and cooling, both the strip and the lamina undergo the same curvature X. The following moment-curvature relations are assumed:

$$\text{SMA strip} \qquad m_{\mathrm{S}} = E_{\mathrm{S}} I_{\mathrm{S}} (\mathrm{X} - \mathrm{X}_0), \tag{4.1}$$

$$\text{Polymeric lamina} \qquad m_{\mathrm{P}} = E_{\mathrm{P}} I_{\mathrm{P}} \mathrm{X}, \tag{4.2}$$

where X_0 is the curvature that the SMA strip would attain in the recovery-free condition, E_S and E_P are the elastic moduli of the SMA and of the polymer, respectively, and I_S and I_P are the second moment of inertia of the SMA strip and of the polymeric lamina cross-sections, respectively. In Eqs. (4.1) and (4.2) and in the rest of the paper, the subscripts S and P denote quantities associated with the SMA strip and with the polymeric lamina, respectively.

Due to the martensitic phase transformation, the elastic modulus of the SMA material, E_S, is expected to be temperature dependent. The classical rule of mixtures is adopted:

$$E_{\mathrm{S}}(\mathrm{T}) = \xi(\mathrm{T}) E_{\mathrm{M}} + (1 - \xi(\mathrm{T})) E_{\mathrm{A}}, \tag{4.3}$$

where E_A and E_M are the austenite and the martensite elastic moduli, respectively, and $\xi(T)$ is the martensite volume fraction linearly dependent upon the temperature according to the following simple kinetic law:

$$\xi(\mathrm{T}) = \begin{cases} \frac{(\mathrm{A_F}-\mathrm{T})}{(\mathrm{A_F}-\mathrm{A_S})}, & \mathrm{A_S} \le \mathrm{T} \le \mathrm{A_F}, \dot{\mathrm{T}} > 0 \quad \text{(on heating)}, \\ \frac{(\mathrm{M_S}-\mathrm{T})}{(\mathrm{M_S}-\mathrm{M_F})}, & \mathrm{M_F} \le \mathrm{T} \le \mathrm{M_S}, \dot{\mathrm{T}} < 0 \quad \text{(on cooling)}. \end{cases} \tag{4.4}$$

At equilibrium, the net bending moment vanishes:

$$0 = m_\mathrm{S} + m_\mathrm{P} = E_\mathrm{S} I_\mathrm{S} (\mathrm{X} - \mathrm{X}_0) + E_\mathrm{P} I_\mathrm{P} \mathrm{X}, \tag{4.5}$$

implying:

$$\mathrm{X} = \frac{E_\mathrm{S} I_\mathrm{S} \mathrm{X}_0}{(E_\mathrm{S} I_\mathrm{S} + E_\mathrm{P} I_P)}. \tag{4.6}$$

From Fig. 5 it follows that the curvature X_0 evolves with the number of cycles and, due to the training of the SMA material, it takes different values at high temperature (105 °C) and low temperature (35 °C).

In order to describe the controlled recovery behavior investigated in Section 3, we briefly recall some results obtained by Brinson for the simulation of controlled recovery in a SMA wire [48] (cf. also [49,54]). According to Brinson's model, the stress-temperature diagram with the relation (solid lines) between the stress and the temperature during controlled recovery in a SMA strip placed in series with a linear spring is depicted in Fig. 8. While the classic stress-temperature diagram (cf. [55,56]) considers only the presence of two phases, A and M, this extended diagram proposed by Brinson considers the presence of three phases, twinned martensite (S), detwinned martensite (M) and austenite (A). Another feature of this diagram is the assumption that the critical stresses σ_S, σ_F are independent of the temperature in the range (M_F, M_S).

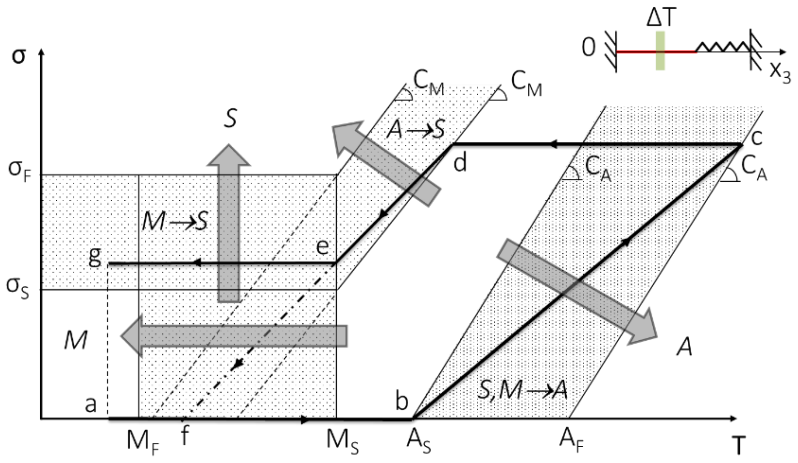

Figure 8 – Relation between stress and temperature during uniaxial controlled recovery in a SMA wire. Gray arrows indicate the direction of phase production.

According to Fig. 8, the transformation (A→S) interrupts at T= M_S and further cooling below M_S induces only the transformation (A→M). Because the latter transformation occurs without any apparent change of shape (due to self-accommodation), the complete recovery of the deformation is prevented, thus resulting in a residual deformation of the SMA material and a residual stress inside the structure at the end of cooling (point "g" in Fig. 8).

In view of Brinson's simulation of uniaxial controlled recovery, for the theoretical prediction of the bending behavior of the SMA-based beam we assume that, during cooling, the curvature recovery stops at M_S. For the 1st actuation cycle (which would be the 51st training cycle), X_0 is thus assumed to be given by the 50th training cycle with the additional hypothesis that on cooling X_0 is constant below M_S and equal to X_0 (M_S) (cf. Fig. 9a). Analogously, for the 2nd actuation cycle (which would be the 52nd training cycle), the evolution of X_0 is shown in Fig. 9b: on heating, X_0 is constant and equal to X_0 (M_S) up to the ascending branch of the 50th

training cycle; on cooling, X_0 follows the 50th training cycle down to M_S and it is constant and equal to X_0 (M_S) below M_S.

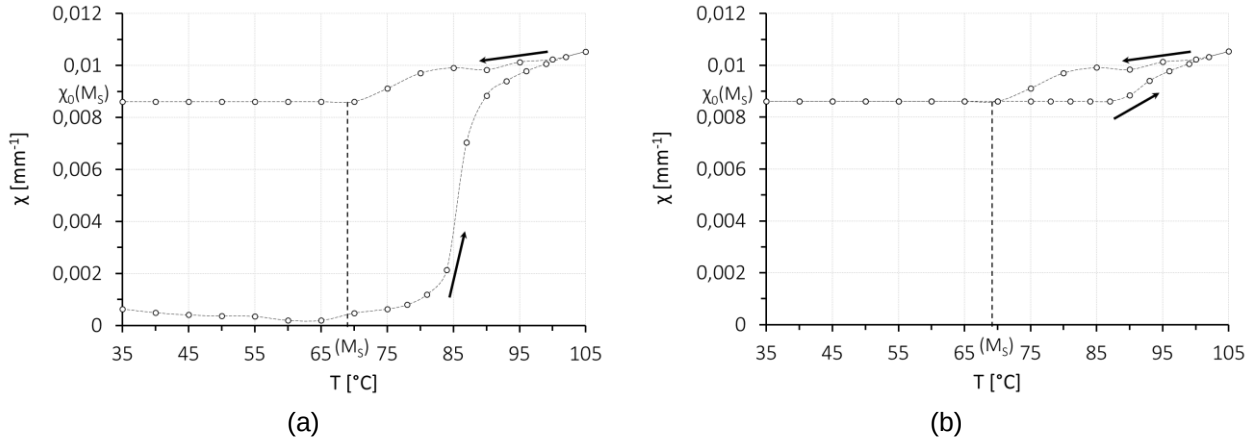

Figure 9 – Modified curvature-temperature evolution of the 50th training cycle: (a) adopted to model the 1st actuation cycle and (b) adopted to model the 2nd actuation cycle.

The curvature X is related to the deformed shape of the structure described in a Cartesian coordinate system by the equations:

$$\begin{aligned} \frac{d\varphi}{ds} &= \mathrm{X}, & \varphi(0) &= 0, \\ \frac{d\mathrm{w}}{ds} &= \cos\varphi - 1, & \mathrm{w}(0) &= 0, \\ \frac{d\mathrm{v}}{ds} &= -\sin\varphi\,, & \mathrm{v}(0) &= 0, \end{aligned} \tag{4.7}$$

with $s \in [0, L]$ denoting the arc-length coordinate of the mean line, φ, w and v are the angular rotation, the axial and the transversal displacements along the deformed length of the structure. Substituting Eq. (4.6) into Eq. (4.7) and integrating, the following relations are obtained:

$$\begin{aligned} \varphi(s) &= \mathrm{X}s, \\ \mathrm{w}(s) &= \frac{1}{\mathrm{X}}\sin(\mathrm{X}s) - s, \\ \mathrm{v}(s) &= \frac{1}{\mathrm{X}}[\cos(\mathrm{X}s) - 1]. \end{aligned} \tag{4.8}$$

In view of Eq. (4.6) and (4.8), the predicted deflection at the arc-length *s* is:

$$v(s) = \frac{(E_S I_S + E_P I_P)}{E_S I_S \mathrm{X}_0}\left[1 - \cos\left(\frac{E_S I_S \mathrm{X}_0}{(E_S I_S + E_P I_P)}\mathrm{s}\right)\right], \tag{4.9}$$

with X_0 given by the diagram depicted in Fig. 9a for the 1st actuation cycle and by the diagram depicted in Fig. 9b for the 2nd actuation cycle.

5. Experimental verification

The validation study of the proposed model is presented herein by comparing experimental findings with the analytical solutions. Preliminary, experimental data of the SMA strip training cycles are considered. The evolution of the maximum curvature (at 105 °C) and the residual curvature (at 35 °C), as a function of the training cycles, N, are given in Fig. 10. Both maximum and residual curvature data decrease as the number of cycles increases and, due to the thermomechanical loading, they display an asymptotic behavior. Considering the assumption that, on cooling, the curvature recovery stops at M_S, the curvature data correspondent to the martensitic finish temperature X_0(M_S) are represented. As expected, these data show the same asymptotic behavior of maximum and residual curvatures and are slightly lower than the maximum ones due to the SMA phase transformation.

In view of Eq. (4.8), the transversal displacement at the beam's tip is dependent on the curvature X, which in turn is a function of X_0 as indicated by Eq. (4.6). For the curvature X_0, the following phenomenological expressions have been assumed:

$$\mathrm{X}_0\ (105\ °C, N) \approx 0.011 + 0.018e^{(-N/9.295)}, \tag{5.1}$$

$$\mathrm{X}_0\ (\mathrm{M_S}, N) \approx 0.009 + 0.020e^{(-N/8.156)}, \tag{5.2}$$

$$\mathrm{X}_0\ (35\ °C, N) \approx 0.003 + 0.019e^{(-N/9.516)}, \tag{5.3}$$

obtained from the least squares fitting procedure applied to the experimental data of the training cycles (cf. Fig. 10).

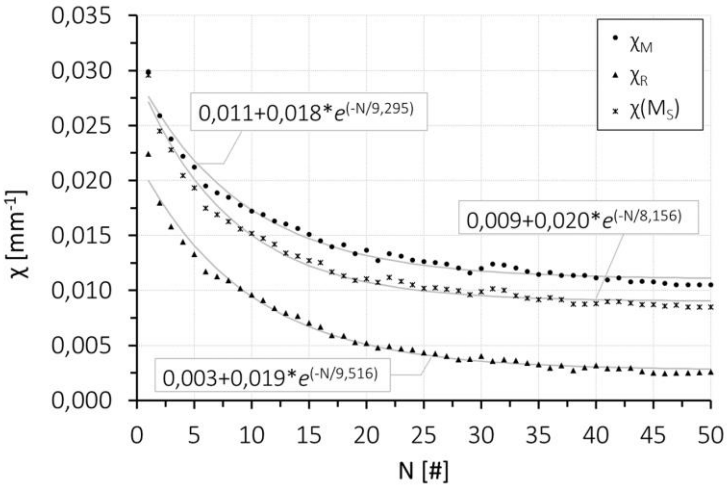

Figure 10 – Curvature vs. training cycles: comparison among data of maximum curvature, residual curvature and curvature measured at the martensitic finish temperature.

Moreover, in the present model, the dependence of the elastic moduli on temperature has been considered for both the SMA material and the polymeric compound (cf. Eq. (4.6)). For the SMA strip E_M and E_A have been experimentally determined (cf. Tab. 1) and a dependence of the SMA elastic modulus, E_S, upon the temperature has been assumed via Eqns. (4.3) and (4.4). For the polymeric lamina the dependence of tensile modulus upon the temperature has been evaluated consistently with literature data. According to [57], Fig. 11 provides the evolution of E_P with increasing temperature for a PA66-GF30 conditioned at 50 % relative humidity. This dependence has been chosen considering the following boundary conditions and in accordance with the moisture absorption curve of the material: (i) thickness of the injected molded plate, (ii) conditioning at 23 °C and 50 % relative humidity and (iii) moisture absorption at the equilibrium. Based on the reported trend, E_P values at 35 °C and 105 °C have been estimated as 6300 MPa and 4000 MPa, respectively.

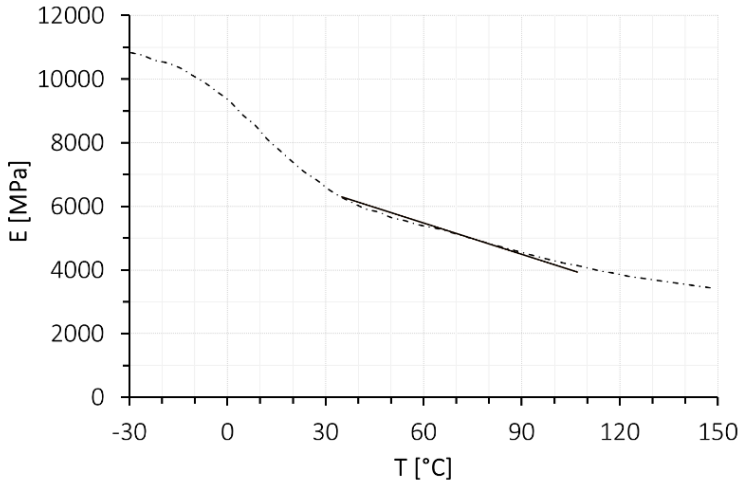

Figure 11 – Tensile modulus vs. temperature for a 30 % glass fiber reinforced PA66 resin conditioned at 50 % relative humidity. Adapted from [57].

To model the dependence of E_P upon the temperature, we assume the following linear variation

$$E_P(\mathrm{T}) = 32{,}85(35 - \mathrm{T}) + 6300 \ \ \text{(MPa)}, \tag{5.4}$$

showing a good agreement with the data extrapolated from Fig.11 in the temperature range between M_s and 105 °C (cf. solid line in Fig. 11).

Figure 12 displays the comparison between experimental data and theoretical prediction of the curvature-temperature diagrams for the 1st (Fig. 12a) and 2nd (Fig. 12b) actuation cycles. Even though the results obtained for the 1st actuation cycle show some differences with respect to the experimental data during the cooling phase, the comparison indicates a good agreement.

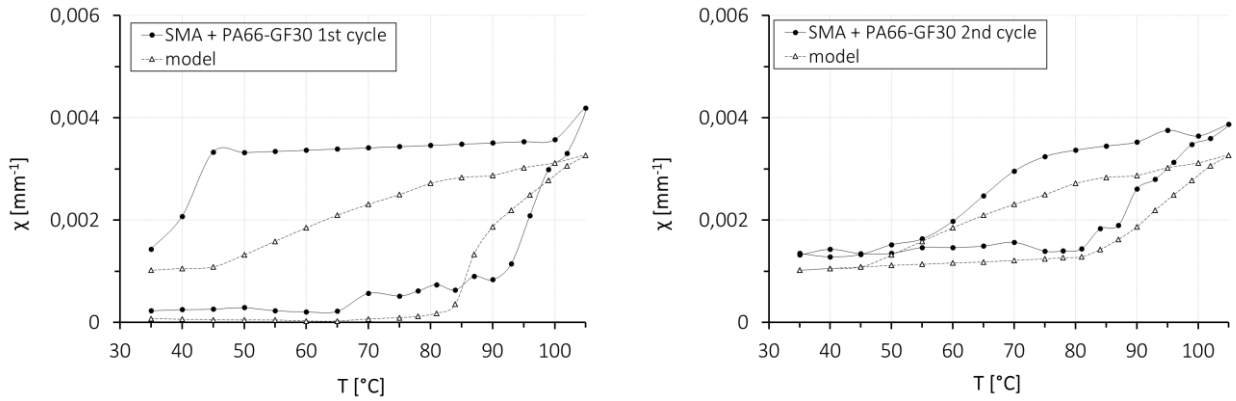

Figure 12 – Curvature-temperature evolution for the 1st and 2nd thermal actuation cycles: experimental and theoretical prediction.

In addition to the curvature trends, the deflections data have also been evaluated. In view of Eq. (4.9), the deflection at the beam's tip at the end of the heating (105 °C) and at the end of cooling (35 °C) ramps are given by the relations:

$$\delta(105°C, N) = -\frac{(E_S I_S + E_P I_P)}{E_S I_S \mathrm{X}_0(105°C, N)}\left[1 - \cos\left(\frac{E_S I_S \mathrm{X}_0(105°C, N)\, L}{(E_S I_S + E_P I_P)}\right)\right], \tag{5.5}$$

$$\delta(35°C, N) = -\frac{(E_S I_S + E_P I_P)}{E_S I_S \mathrm{X}_0(\mathrm{M_S}, N)}\left[1 - \cos\left(\frac{E_S I_S \mathrm{X}_0(\mathrm{M_S}, N)\, L}{(E_S I_S + E_P I_P)}\right)\right], \tag{5.6}$$

respectively. Notably, the deflection obtained with Eq. (5.6) is greater than the one obtained by considering X_0 evaluated at 35 °C. Again, this is related to the fact that the direct transformation ($A \rightarrow S$) is assumed to stop at M_S, implying that a smaller curvature recovery occurs on cooling.

Tip beam deflections resulting from Eqns. (5.5) and (5.6) are now compared with the experimental data from actuation cycles. Figure 13 provides both the maximum/residual deflections trends (solid diamond and solid square markers, respectively) and the predicted values (open diamond and open square markers, respectively). As noted, the experimental deflection shows a stable and repeatable behavior with increasing the number of actuation cycles, n. In addition, from the comparison between analytical solutions and experimental findings, it emerges that the proposed theoretical prediction provides a quantitative description of the SMA-based structure deflections.

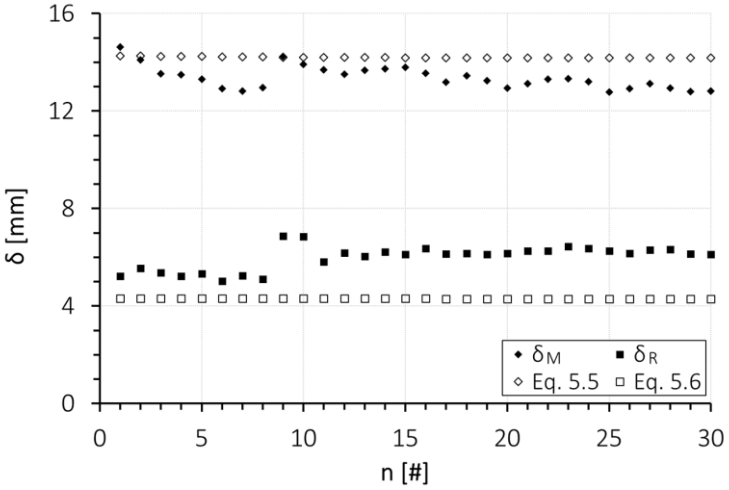

Figure 13 – Tip beam deflection vs actuation cycles: experimental and numerical prediction at the end of the heating ramp (T = 35 °C) and at the end of the cooling ramp (T = 105 °C).

Finally, to completely characterize the bending behavior of the structure, the deflection along the entire SMA-based beam is also considered. Figure 14 displays the experimental and the predicted maximum (Fig. 14a) and residual (Fig. 14b) deflection trends for the 1st actuation cycle. The experimental deflections have been calculated by digital image analysis, considering the markers located at 0, ¼ L, ½ L, ¾ L and L (crossed markers displayed in Fig. 14) fitted by a fourth-order polynomial (solid lines in Fig. 14) and compared with the predicted deflection given by Eq. (4.9). The superimposition between the above-described deflections and the related video frames at 105 °C (Fig. 14a) and 35 °C (Fig. 14b) show the accuracy of the proposed model.

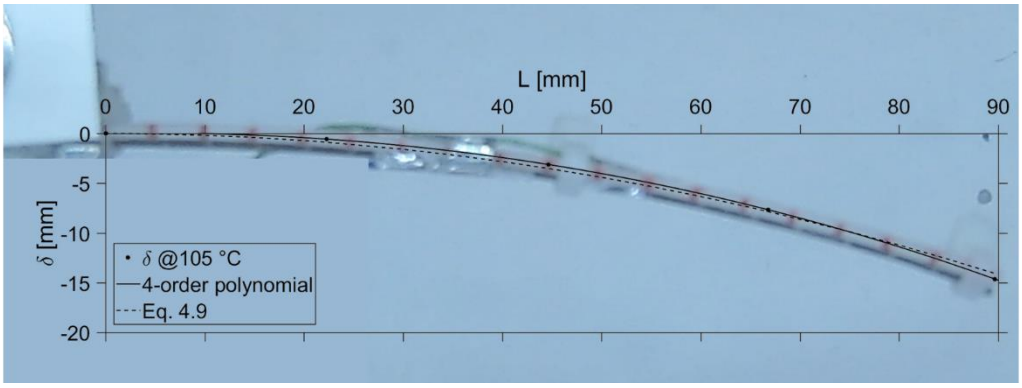

(a)

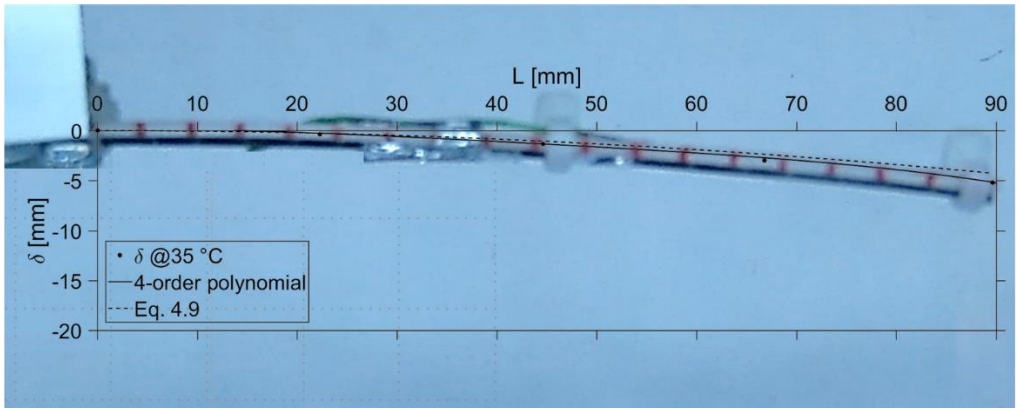

(b)

Figure 14 – Superimposition of both experimental and predicted deflections at the 1st actuation cycle along the beam length with the video frame at (a) 105 °C and (b) 35 °C.

6. Discussion

The goal of this paper is the development of an easy and practical approach to the design of active SMA-based structures working in bending. The good agreement between theoretical predictions and experimental findings indicates that the proposed model can be effectively used to study the repeatable bending actuation of a SMA-based cantilevered beam.

As for the experimental outcomes, it has been proven that the airflow thermal actuation, via controlled heating and cooling ramps, can be successfully adopted to promote the SMA strip phase transformations (cf. Fig. 4). This solution prevents, among others, the heat transfer issues associated with electrical actuation, which is not always as feasible as it might seem [58]. In addition, such an approach, initially intended by the authors for experimentally testing a SMA-based morphing blade [59], has been established as a reliable one by considering the constant monitoring during actuation. Other experimental works have already evaluated the bending behavior of SMA-based elements through the assessment of the curvature-temperature trends [60–62]. Nevertheless, the CAD reconstruction via digital image analysis proposed in the present paper and performed by means of several measurement points during actuation, provides a detailed and comprehensive description of the bending. Considering the thermomechanical training, Fig. 5 shows a noticeable shift of the curvature-temperature evolution between the first and the subsequent cycles on heating. In particular, the M→A phase transformation temperatures, starting from the 10th cycle, are 10 °C lower compared to the ones of the first heating ramp. Such a behavior is consistent with the experimental findings reported in [63,64]. Moreover, a saturated hysteretic response of the NiTi alloy after about 30 cycles is observed. According to the literature, the hysteretic behavior of SMAs, i.e. due to the SME, stems from internal friction generated by the movement of the A-M interface and the associated structural defects [65]. Noticeably, the firsts thermomechanical cycles entail the accumulation of plastic strain, even if training promotes the progressive stabilization of such strains and the reduction of the non-closed hysteretic loops. In addition, thermomechanical cycling promotes the rise of the deviation between X_M and X_R on increasing the number of cycles (Fig. 10). The evolution of hot and cold shapes suggests that, apart from the 30 first cycles where a gradual loss in the memorized shape occurs, the hot shape is progressively stabilized. Besides, the cold shape gradually evolves towards the flat one and hence the difference between hot and cold shapes is maximized. These experimental findings suggest that, apart from the desired SME stabilization, thermomechanical training cycles promote the two-way shape memory effect (TWSME), as indicated from the increasing difference between hot and cold shapes on increasing the number of training cycles. Such a difference, sometimes referred to as two-way recoverable shape change, provides an indication of the TWSME over training [63]. As it usually occurs when SMAs are adopted in actuation devices, training enables to prevent any drift in the hysteresis during the subsequent thermal actuation cycles. In this regard, the tip beam deflections against actuation thermal cycles show a stable and repeatable behavior for both maximum and residual data. These trends indicate that after 50 training cycles the thermomechanical behavior of the structure is stabilized and that the PA66-GF30 lamina shows an elastic behavior. Such actuations were conducted within the same temperature range employed for the training cycles. Therefore, considering the TTRs of the material determined by DSC tests for the material in the stress-free condition (cf.

Tab.1), a partially M→A phase transformation would occur. Given that temperature and applied stress have mutual effects on the transformation mechanisms, i.e. on TTRs, the hysteresis loop in presence of the polymer lamina is shifted to the right with respect to the stress-free cycle (cf. Fig. 7). While the SMA strip response in the stress-free condition depends basically on the shape-setting process, on the detwinning condition and on the actuation temperature, on the other hand, the bending behavior of the SMA-based structure relies on the SMA strip thermomechanical training, on the polymeric lamina stiffness and on the austenite phase fraction occurring at the end of the heating ramp. As a result, given that the actuation was performed in the range of 35 °C – 105 °C, the SMA-based beam reaches a maximum curvature value, which is reduced by 60 % with respect to the 50th training cycle. By contrast, considering that the experimental deflections of the structure are of about 15 mm (cf. solid markers of Fig. 13), it follows that the PA66-GF30 provides both the expected elasticity to promote macroscopic deformations on heating and the proper stiffness on cooling.

Concerning the theoretical prediction, we note that the diagrams depicted in Fig. 9 give rise to a simple phenomenological model which is unable to simulate the martensite and austenite phase distributions along the cantilever. However, the comparison between the experimental and the predicted deflections along the beam, for both maximum and residual conditions evaluated at the 1st actuation cycle (Fig. 14), indicates that the proposed modeling approach is accurate enough for the study of the overall behavior. Moreover, the experimental data on the heating phase of the 1st actuation cycle, whereas it shows some differences in comparison with the experimental response on cooling (Fig. 12a). For the 2nd actuation cycle, the agreement is very good (Fig. 12b). In controlled recovery conditions, an incomplete shape recovery has been already previously reported in other works [17,19,34,60,62], where a residual tip deflection or an incomplete curvature recovery are observed at the end of cooling. In [34], smart composite beams embedded with prestrained Nitinol wire actuators were developed. Both single-cycle and multi-cycle thermomechanical bending actuations of these structures in the cantilever set-up were characterized experimentally by applying various levels of electric current to the nitinol wires. The residual tip deflection detected at the end of cooling was attributed to the difference between M_F and room temperature, so that the forward transformation was likely to be incomplete. In particular, the actual M_F of the prestrained wires was supposed to be less than that tested with zero prestrain. In [60], the design of a reversible bending actuator made of SMA NiTi embedded in a shape recovery polymer matrix with a memorized flat shape is presented. The occurrence of incomplete recovery has been attributed to the residual strain stored by the (shape memory) polymer once that the temperature drops far enough below the glass transition temperature such that fixation occurs. In [62], SMA composites were manufactured using NiTi wires and woven glass fiber pre-impregnated fabrics. The experimental data of actuation showed reasonable agreement with an analytical solution proposed to investigate the curvature achievable during actuation. A residual curvature was observed and it was attributed to some undetected residual heat in the samples after cooling at the end of each cycle.

Another possible cause of incomplete recovery at the end of cooling could be the occurrence of plastic deformation in the SMA-based structure, both in the polymeric strip or in the SMA material. As already remarked, the stable and repeatable behavior observed for both maximum and residual tip deflection in our SMA-coupled structure (cf. Fig. 13) is in favor of an elastic behavior of the PA66-GF30 lamina. Therefore, our results seem to attribute the incomplete curvature recovery to the stop of the transformation (A→S) at T= M_S. Other effects, due for example to the variation of M_f or residual heat in the structure at the end of cooling are not taken into account by the proposed model. These and other aspects will be the object of further study.

7. Conclusions

In this work, theoretical prediction and experimental validation of the bending deformations occurring in a SMA-based cantilevered beam, actuated via airflow heating/cooling ramps in a purpose-built test bench, are reported. The main goal is to investigate the bending behavior of such active deformable structures and to provide a simple and effective design approach.

Thermomechanical training of the SMA strip and actuation cycles of the SMA-based structure, made up of a SMA strip externally joined to a PA66-GF30 polymeric lamina, have been quantitatively analyzed considering both deflections and curvature trends. Based on the experimental findings and on the simulation of controlled recovery in traction proposed by Brinson [48], an analytical description of the bending behavior of the SMA-based structure has been presented. Considering the main experimental and analytical outcomes, the following concluding remarks can be made:

- The shape-setting treatment of the SMA material enables to memorize the proper bent shape and the 50 training cycles of the SMA strip resulted in an effective curved shape able to promote the deflection during the subsequent actuation cycles. Thermomechanical training, performed by controlled deformations at a temperature below M_F followed by heating/cooling ramps from below M_F up to above A_F, enabled to go beyond the unstable properties of SMA in early loading cycles. A gradual stabilization and the repeatability of the SME up to about 30 thermomechanical training cycles have been observed;
- The externally joining of SMA strip to the polymeric lamina, coupled with the airflow actuation mode, have proven to be an effective solution to study the bending behavior of the structure, resulting from the temperature-induced phase changes of the SMA strips;
- The experimental trends of the SMA-based structure showed a stable and repeatable behavior for both the maximum deflection data, i.e. at the end of heating, and for the residual deflection data, i.e. at the end of the actuation cycle (cf. Fig. 13). These trends indicate the effectiveness of the thermomechanical training and that the PA66-GF30 lamina actually provides both the expected elasticity to promote macroscopic deformations on heating and the proper stiffness on cooling;
- Based on Brinson's model, the recovery of the bending deformation on cooling has been assumed to stop at M_S and the curvature-temperature diagrams for the 1st and 2nd actuation cycles have been simulated;
- The theoretical predictions of the bending behavior of the SMA-based structure in controlled recovery conditions show good agreement with the experimental findings, revealing the good predictive capability of the proposed model able to quantitatively describe the deflection of the structure.

With the objective of highlighting the main physical principles underlying the SMA-based structure behavior, the present study is expected to provide simple but effective equations to be used for the design of such structures. Indeed, the proposed analytical method simulates the bending behavior of a SMA-based flexible beam, with a low computational cost and relatively basic implementation. Such an approach, starting from a simple SMA-based beam in the cantilevered condition, provides to practitioners and engineers an easy-to-use analysis, which opens for practical implementations and optimized exploitation of SMAs. Starting from these considerations, the analysis could be extended to more SMA-polymer configurations for the optimization of aerodynamic flexible structures with several modes of actuation. The improvement in the knowledge of SMAs behavior would thus reflect towards the increase of their performance and, in turn, of their application ranges.

9. References

[1] Lester B, Baxevanis T, Chemisky Y and Lagoudas D 2015 Review and Perspectives : Shape Memory Alloy Composite Systems *Acta Mech.* **226** 3907–60

[2] Rodrigue H, Wang W, Han M and Kim T J Y 2017 An Overview of Shape Memory Alloy-Coupled Actuators and Robots *Soft Robot.* **4** 1–13

[3] Lecce L and Concilio A 2015 *Shape Memory Alloy ENGINEERING for Aerospace, Structural and Biomedical Applications* (Butterworth-Heinemann)

[4] Lagoudas D C 2008 *Shape Memory Alloys* (Springer)

[5] Costanza G, Tata M E and Calisti C 2010 Nitinol one-way shape memory springs: Thermomechanical characterization and actuator design *Sensors Actuators, A Phys.* **157** 113–7

[6] Dhakal B, Nicholson D E, Saleeb A F, Padula S A I and Vaidyanathan R 2016 Three-dimensional deformation response of a NiTi shape memory helical-coil actuator during thermomechanical cycling : experimentally validated numerical model *Smart Mater. Struct.* **25** 1–16

[7] Auricchio F, Scalet G and Urbano M 2014 A numerical/experimental study of nitinol actuator springs *J. Mater. Eng. Perform.* **23** 2420–8

[8] Yang K and Gu C L 2008 A compact and flexible actuator based on shape memory alloy springs *Proc. Inst. Mech. Eng. Part C J. Mech. Eng. Sci.* **222** 1329–37

[9] Shim J, Quan Y, Wang W, Rodrigue H, Song S and Ahn S 2015 A smart soft actuator using a single shape memory alloy for twisting actuation *Smart Mater. Struct.* **24** 125033

[10] Kim C, Park B-S and Goo N-S 2002 Shape changes by coupled bending and twisting of shape-memory-alloy-embedded composite beams *Smart Mater. Struct.* **11** 519–26

[11] Feng N, Liu L, Liu Y and Leng J 2015 Characteristics of multi-functional composites using elastomer embedded with Shape Memory Alloy wires *Mater. Des.* **88** 75–81

[12] Eshghinejad A, Elahinia M and Goel V K 2013 Functionality Evaluation of a Novel Smart Expandable Pedicle Screw to Mitigate Osteoporosis Effect in Bone Fixation : Modeling and Experimentation *Smart Mater. Res.* **2013**

[13] Duerig T, Pelton A and Stöckel D 1999 An overview of nitinol medical applications *Mater. Sci. Eng. A* **273**–**275** 149–60

[14] Chopra I 2000 Status of Application of Smart Structures Technology to Rotorcraft Systems *J. Am. Helicopter Soc.* **45** 228–52

[15] Turner T L, Buehrle R D, Cano R J and Fleming G A 2006 Modeling, fabrication, and testing of a SMA hybrid composite jet engine chevron concept *J. Intell. Mater. Syst. Struct.* **17** 483–97

[16] Fortini A, Suman A, Merlin M and Garagnani G L 2015 Morphing blades with embedded SMA strips: An experimental investigation *Mater. Des.* **85** 785–95

[17] Baz A, Chen T and Ro J 2000 Shape control of NITINOL-reinforced composite beams *Compos. Part B* **31** 631–42

[18] Tobushi H, Pieczyska E A, Nowacki W K, Sakuragi T and Sugimoto Y 2009 Torsional deformation and rotary driving characteristics of SMA thin strip *Arch. Mech.* **61** 241–57

[19] Gao X, Burton D, Turner T L and Brinson L C 2006 Finite element analysis of adaptive-stiffening and shape-control SMA hybrid composites *J. Eng. Mater. Technol.* **128** 285–93

[20] Jani J M, Leary M, Subic A and Gibson M A 2014 A review of shape memory alloy research, applications and opportunities *Mater. Des.* **56** 1078–113

[21] Kalra S, Bhattacharya B and Munjal B S 2017 Design of Shape Memory Alloy Actuated Intelligent Parabolic Antenna for Space Applications *Smart Mater. Struct.* **26** 1–14

[22] Hartl D J and Lagoudas D C 2007 Aerospace applications of shape memory alloys *Proc. Inst. Mech. Eng. Part G J. Aerosp. Eng.* **221** 535–52

[23] Barbarino S, Saavedra Flores E L, Ajaj R M, Dayyani I and Friswell M I 2014 A review on shape memory alloys with applications to morphing aircraft *Smart Mater. Struct.* **23**

[24] Janke L, Czaderski C, Motavalli M and Ruth J 2005 Applications of shape memory alloys in civil engineering structures - Overview, limits and new ideas *Mater. Struct. Constr.* **38** 578–92

[25] Saadat S, Salichs J, Noori M, Hou Z, Davoodi H, Suzuki Y and Masuda A 2002 An overview of vibration and seismic applications of NiTi shape memory alloy *Smart Mater. Struct.* **11** 218–29

[26] Biesiekierski A, Wang J, Abdel-Hady Gepreel M and Wen C 2012 A new look at biomedical Ti-based shape memory alloys *Acta Biomater.* **8** 1661–9

[27] Petrini L and Migliavacca F 2011 Biomedical Applications of Shape Memory Alloys *J. Metall.* **2011** 1–15

[28] El Feninat F, Laroche G, Fiset M and Mantovani D 2002 Shape memory materials for biomedical applications *Adv. Eng. Mater.* **4** 91–104

[29] Rodrigue H, Wang W, Bhandari B, Han M and Ahn S 2015 SMA-based smart soft composite structure capable of multiple modes of actuation *Compos. Part B* **82** 152–8

[30] Epps J and Chandra R 1997 Shape memory alloy actuation for active tuning of composite beams *Smart Mater. Struct.* **6** 251–64

[31] Chandra R 2001 Active shape control of composite blades using shape memory actuation *Smart Mater. Struct.* **10** 1018–24

[32] Yang S-M, Roh J-H, Han J-H and Lee I 2006 Experimental Studies on Active Shape Control of Composite Structures using SMA Actuators *J. Intell. Mater. Syst. Struct.* **17** 767–77

[33] Schrooten J, Michaud V and Parthenios J 2002 Progress on composites with embedded shape memory alloy wires *Mater. Trans.* **43** 961–73

[34] Zhou G and Lloyd P 2009 Design, manufacture and evaluation of bending behaviour of composite beams embedded with SMA wires *Compos. Sci. Technol.* **69** 2034–41

[35] Sadrnezhaad S K, Nemati N H and Bagheri R 2009 Improved adhesion of NiTi wire to silicone matrix for smart composite medical applications *Mater. Des.* **30** 3667–72

[36] Merlin M, Scoponi M, Soffritti C, Fortini A, Rizzoni R and Garagnani G L 2015 On the improved adhesion of NiTi wires embedded in polyester and vinylester resins *Frat. ed Integrita Strutt.* **31** 127–37

[37] Neuking K, Abu-Zarifa A and Eggeler G 2008 Surface engineering of shape memory alloy/polymer-composites: Improvement of the adhesion between polymers and pseudoelastic shape memory alloys *Mater. Sci. Eng. A* **481**–**482** 606–11

[38] Jonnalagadda K, Kline G and Sottos N 1997 Local displacement and load transfer in shape memory alloy composites *Exp. Mech.* **37** 78–86

[39] Lei H, Wang Z, Tong L, Zhou B and Fu J 2013 Experimental and numerical investigation on the macroscopic mechanical behavior of shape memory alloy hybrid composite with weak interface *Compos. Struct.* **101** 301–12

[40] Shakeri M S and Aghajani H 2013 Modeling of stress relaxation process, case study: Shape setting heat treatment of a Ni rich-NiTi alloy *J. Alloys Compd.* **574** 119–23

[41] Rao A, A R S and Reddy J N 2015 *Design of Shape Memory Alloy (SMA) Actuators* (Springer)

[42] Rizzoni R, Merlin M and Casari D 2013 Shape recovery behaviour of NiTi strips in bending: Experiments and modelling *Contin. Mech. Thermodyn.* **25** 207–27

[43] Morgan N B and Broadley M 2003 Taking the art out of smart! - Forming processes and durability issues for the application of NiTi shape memory alloys in medical devices *Medical Device Materials: Proceedings of the Materials & Processes for Medical Devices Conference* ed S Shrivastava (ASM International) pp 247–52

[44] Pittaccio S and Garavaglia L 2014 Electric resistance monitoring as a method for controlling shape memory alloy characteristics during shape-setting treatments in the furnace *Mater. Sci. Eng. A* **599** 92–104

[45] Merlin M, Soffritti C and Fortini A 2011 Study of the heat treatment of NiTi shape memory alloy strips for the realisation of adaptive deformable structures *Metall. Ital.* 17–21

[46] Fortini A, Merlin M, Soffritti C, Suman A and Garagnani G L 2015 Study of an active deformable structure with embedded niti shape memory alloy strips *La Metall. Ital.* 23–30

[47] Cisse C, Zaki W and Zineb T Ben 2016 A review of modeling techniques for advanced effects in shape memory alloy behavior *Smart Mater. Struct.* **25** 1–36

[48] Brinson L C 1993 One-dimensional constitutive behavior of shape memory alloys: Thermomechanical derivation with non-constant material functions and redefined martensite internal variable *J. Intell. Mater. Syst. Struct.* **4** 229–42

[49] Auricchio F and Sacco E 1999 A temperature-dependent beam for shape-memory alloys: Constitutive modelling, finite-element implementation and numerical simulations *Comput. Methods Appl. Mech. Eng.* **174** 171–90

[50] Evangelista V, Marfia S and Sacco E 2009 Phenomenological 3D and 1D consistent models for shape-memory alloy materials *Comput. Mech.* **44** 405–21

[51] Ben Jaber M, Smaoui H and Terriault P 2008 Finite element analysis of a shape memory alloy three-dimensional beam based on a finite strain description *Smart Mater. Struct.* **17**

[52] Fortini A, Suman A, Aldi N, Merlin M and Pinelli M 2016 A Shape Memory Alloy-Based Morphing Axial Fan Blade - Part I : Blade Structure Design and Functional Characterization *J. Eng. Gas Turbines Power* **138** 1–8

[53] Suman A, Fortini A, Aldi N, Merlin M and Pinelli M 2016 A Shape Memory Alloy-Based Morphing

Axial Fan Blade - Part II: Blade Shape and Computational Fluid Dynamics Analyses *J. Eng. Gas Turbines Power* **138** 1–9

[54] Marfia S and Rizzoni R 2013 One-dimensional constitutive SMA model with two martensite variants: Analytical and numerical solutions *Eur. J. Mech.* **40** 166–85

[55] Kosel F and Videnic T 2007 Generalized plasticity and uniaxial constrained recovery in shape memory alloys *Mech. Adv. Mater. Struct.* **14** 3–12

[56] Videnic T, Brojan M, Kunavar J and Kosel F 2014 A Simple One-Dimensional Model of Constrained Recovery in Shape Memory Alloys *Mech. Adv. Mater. Struct.* **21** 376–83

[57] McKeen L W 2008 *The effect of temperature and other factors on plastics and elastomer* (Elsevier)

[58] Ramaiah K V, Saikrishna C N, Ranganath V R, Buravalla V and Bhaumik S K 2011 Fracture of thermally activated NiTi shape memory alloy wires *Mater. Sci. Eng. A* **528** 5502–10

[59] Suman A, Fortini A, Aldi N, Pinelli M and Merlin M 2015 Using shape memory alloys for improving automotive fan blade performance: experimental and computational fluid dynamics analysis *Proceedings of the Institution of Mechanical Engineers, Part A: Journal of Power and Energy* vol 229pp 477–86

[60] Taya M, Liang Y, Namli O C, Tamagawa H and Howie T 2013 Design of two-way reversible bending actuator based on a shape memory alloy / shape memory polymer composite *Smart Mater. Struct.* **22**

[61] Dahnke C, Shapovalov A and Tekkaya A E 2017 Thermally activated lightweight actuator based on hot extruded Thermally activated metal lightweight based on hot extruded shape memory matrix actuator composites shape memory metal matrix composites (SMA-MMC) *Procedia Eng.* **207** 1511–6

[62] Naghashian S, Fox B L and Barnett M R 2014 Actuation curvature limits for a composite beam with embedded shape memory alloy wires *Smart Mater. Struct.* **23**

[63] Luo H Y and Abel E W 2007 A comparison of methods for the training of NiTi two-way shape memory alloy *Smart Mater. Struct.* **16** 2543–9

[64] Abel E, Luo H, Pridham M and Slade A 2004 Issues concerning the measurement of transformation temperatures of NiTi alloys *Smart Mater. Struct.* **13** 1110–7

[65] T W Duerig, K N Melton, D Stöckel C M W 1990 *Engineering Aspects of Shape Memory Alloys* vol 1(Butterworth-Heinemann)